



Investigating the effect of Mn-doped CeO₂ nanoparticles by co-precipitation method

D. Durai Manoharadoss Prabakaran¹ · K. Sadaiyandi² · M. Mahendran³ · Suresh Sagadevan⁴

Received: 24 January 2017 / Accepted: 22 December 2017 / Published online: 9 January 2018
© Springer-Verlag GmbH Germany, part of Springer Nature 2018

Abstract

The paper exhibits a detailed study about the synthesis and characterization in analysis of structural, morphological, optical and electrical investigations of pure and Mn-doped Cerium oxide (CeO₂) nanoparticles which were synthesized by co-precipitation technique. Phase formation of the prepared sample was analyzed with powder X-ray diffraction (PXRD) examines, scanning electron microscopy (SEM) examination. The PXRD comes about affirmed partial crystallinity having cubic phases and the crystallite sizes of the pure and Mn-doped Cerium oxide (CeO₂) were estimated by utilizing Debye–Scherrer’s formula and they were calculated to be 12 and 14 nm individually. SEM pictures revealed that the particles were profoundly accumulated and were of permeable nature. The optical properties of pure and Mn-doped CeO₂ were ascertained by using UV–visible absorption spectrum. The estimated band gap values for the pure and the Mn-doped CeO₂ nanoparticles were observed to be 2.7 and 2.6 eV, respectively, utilizing UV–Vis spectroscopy. At different frequencies and temperatures the dielectric properties of the Mn-doped Cerium oxide (CeO₂) nanoparticles, for example, the dielectric constant, the dielectric loss and the AC conductivity, were studied.

1 Introduction

Nanotechnology is the term used to cover the outline, advancement and use of functional structures with at least one characteristic dimension measured in nanometres. Such materials and systems can be expected to show novel and on a very basic level improved physical, chemical and biological properties, phenomena and processes as a result of the limited size of their constituent particles or molecules. A great amount of consideration has been established by Cerium oxide (CeO₂) nanostructure materials in the recent years. It is because of their unique properties resulting from the low dimensionality and high surface area. They are extensively inspected because of their potential applications,

for example, oxygen sensors, fuel cells, UV absorbents and filters, catalysts, engine exhaust catalysts and polishing materials [1, 2].

With the ultimate objective of synthesizing nano-sized CeO₂ particles with promising control of properties distinctive physical and chemical methods have been studied. Combustion synthesis, spray pyrolysis, microemulsion, semi-batch reactor, sonochemical, mechanochemical and sol–gel [3, 4] are some of the promising controls of the properties. A few studies have been accounted for on the synthesis of metal oxide nanoparticles through the mixed solvothermal method. Synthesis of CeO₂ nanoparticles by homogeneous precipitation in alcohol/water mixed solvents has been analyzed [5]. The synthesized ultrafine CeO₂ nanoparticles by surfactant-mediated precipitation of ceria precursor in acetone/water mixed dissolvable structures have been considered [6]. The manufacture and characterization of mono-scattered CeO₂ nanopowder using ethanol/water system with poly vinylpyrrolidone as stabilizing agent have been studied [7]. The impact of Fe doping CeO₂ on the dielectric constant has been inspected and the result showed that the doped system had a moderately large dielectric constant (ϵ_0) [8]. The examination of the structural, magnetic and optical properties of Ce_{1-x}Co_xO_{2- δ} ($x = 0, 0.02, 0.06, 0.15$ and 0.25) films revealed that their refractive index and extinction coefficient

✉ Suresh Sagadevan
sureshsagadevan@gmail.com

¹ Department of Physics, NPR College of Engineering and Technology, Natham, Dindigul, Tamil Nadu, India

² Department of Physics, Alagappa Government Arts College, Karaikudi, Sivaganga, Tamil Nadu, India

³ Department of Physics, Thiagarajar College of Engineering, Madurai, Tamil Nadu, India

⁴ Department of Physics, AMET University, Chennai 603 112, India

increased with Co concentration [9]. Another review had been made about the structural and magnetic properties of Ni-doped CeO₂ nanoparticles. In this examination it was understood that the lattice parameters which had been figured by using Powder-X software got decreased from 5.41 to 5.40 Å with Ni doping. However, the structure and the optical properties of transition metal (Fe, Co or Ni) doped CeO₂ have been focused less theoretically and there is a scope for further examination [10]. These systems may initiate a various electronic structure and optical properties which may prompt new applications.

The structure and the optical properties of these systems must be examined [11]. Tang et al. [12] researched the redox properties of M-doped CeO₂ (M = Mn, Pr, Sn, Zr) by utilizing first-principles and it was found that the decrease in the O-vacancy formation energy for the Zr-doped CeO₂ was for mostly caused because of the structural distortion, while the diminishing for Mn-, Pr-, or Sn-doped CeO₂ originated from the electronic modification and also from the structural distortion. The impact of Zr doping on the decrease properties of ceria has been reported and it has been accounted for that the Zr dopant could have significant effects on the ceria structure [13]. Analyses have been made on the impacts of Zr and Ti doping on the dielectric response of CeO₂ and the researchers suggested that the ceria–zirconia mixed oxides could have potential use as high-*k* materials in the semiconductor industry [14]. The structural, elastic, electronic and optical properties of cubic ZrO₂-doped CeO₂ (the ceria zirconia mixed oxides) have been less systematically examined and a thorough understanding of the properties of the ceria zirconia mixed oxides at the atomic and electronic levels has not yet been achieved. In this manner, it is significant to analyse the structural, elastic, electronic and optical properties of these systems [15].

In fact, for environmental applications, a new, simplified technique is still required to improve the efficiency of this photocatalyst. The lightweight CeO₂/RGA nanocomposites show improved photo-degradation ability and durability compared with bare CeO₂ nanostructures. The possible mechanism for the photocatalysis of dye degradation and the part of 3D RGO nanosheets were investigated on the basis of these experimental outcomes [16]. Among all the studied metal oxides, CeO₂ has proved to be a promising catalyst because of its strong oxidizing power, high thermal stability, low cost and long-term stability. However, pure metal oxides are produced in large amounts as sludge from these reactions, which is the essential prevention to catalytic applications [17]. Surface oxygen opportunities on Ceria are required to advance effective reactant metal molecule scattering when CeO₂ is used as a support. Under lessening conditions, the abatement of neighboring Ce⁴⁺ particles to Ce³⁺ happens, which supports oxygen opportunity course of action at first look. These Ce³⁺ and oxygen opportunity

can go about as dynamic goals for some synergist responses. Henceforth, the era of surface-oxygen-opportunity rich CeO₂ and its utilization in the amalgamation of CeO₂–AgI nanostructures is a favored system for improving the reactant development of AgI photocatalysis [18].

Manganese has a good optical property and when doped with metal oxides, its composites essentially improve their optical properties. It gives a good magnetic property, when it is doped with some metal oxides and metal sulfides [19]. In low temperature, Mn-doped material behaves as if it is ferromagnetic in nature. Mn-doped materials are seen to be improved in their electrical and dielectric properties. In this paper, the preparation of Mn-doped CeO₂ nanoparticles and their structural, surface morphology, optical and dielectric studies have been studied.

2 Experimental procedure

2.1 Preparation of Mn-doped CeO₂ nanoparticles

All chemical reagents were commercial with AR purity and used directly without further purification. By applying precipitation method pure and Mn-doped CeO₂ nanoparticles were prepared. The required amount of the starting raw materials Ce(NO₃)₃·6H₂O and C₄H₆MnO₄·4H₂O were weighed depending on the percentage of dopant (8 mol%) and dissolved into deionized water. Development of final product is vital to diminish the particle size. For accomplishing this outcome calcining temperature is required. The main reason for this requirement is that co-precipitation method is atomic scale mixing. Homogeneous mixing of reactant precipitates decreases the response temperature. Fulfillment of precipitation was conceivable by gradually adding aqueous ammonium solution with constant stirring until the pH value achieved 10. In order to remove any possible by product the final product was washed a few times with deionized water. The filtrate was at first dried at 80 °C for 12 h and calcined in the temperature range of 600 °C for 5 h in air atmosphere. The prepared powders were carefully subjected to the following characterization studies:

2.2 Characterization techniques

The crystalline size and the structure of the Mn-doped CeO₂ nanoparticles were analyzed by X-ray diffraction (XRD) by using a powder X-ray diffractometer [Schimadzu model: XRD 6000 with CuK_α (λ = 0.154 nm)] radiation and with a diffraction angle between 20° and 60°. By using FTIR model Bruker IFS 66W Spectrometer, the FTIR spectrum of the Mn-doped CeO₂ nanoparticles was obtained. The surface morphology of the Mn-doped CeO₂ nanoparticles was observed with the help of scanning electron microscope

(SEM) using JEOL; JSM- 6701. UV–visible absorption spectrum for the pure and Mn-doped CeO₂ nanoparticles was recorded using a Varian Cary 5E spectrophotometer in the range of 300–900 nm. By using an HIOKI 3532-50 LCR HITESTER in the frequency range of 50 Hz–5 MHz. The dielectric constant and the dielectric loss of the pellets of Mn-doped CeO₂ nanoparticles in disk form were studied at various temperatures.

3 Results and discussion

3.1 Structural analysis

An intense method of X-ray powder diffraction (XRD) was utilized to discover the crystalline phase which is available in materials. It is also useful to measure the structural properties of those phases. X-ray powder diffraction patterns of the pure and the Mn-doped CeO₂ nanoparticles are shown in Fig. 1. The excellent peaks (111), (200), (220), (311), (222), (400), (331) and (422) were obtained. The investigation of peak broadening was required as a result of the tiny grain size of CeO₂ nanoparticles [20]. As the Mn content in CeO₂ nanoparticles increased, the intensity of XRD peaks decreased which demonstrated the degradation of crystallinity. The average grain size of Mn-doped CeO₂ nanoparticles has been determined using the Scherrer formula:

$$D = \frac{0.9\lambda}{\beta \cos \theta}, \quad (1)$$

where λ is the X-ray wavelength, θ is the Bragg diffraction angle and β is the full width at half maximum (FWHM) of the XRD peak appearing at the diffraction angle θ . The average grain sizes of the pure and the Mn-doped CeO₂ nanoparticles were observed to be 12 and 14 nm, respectively.

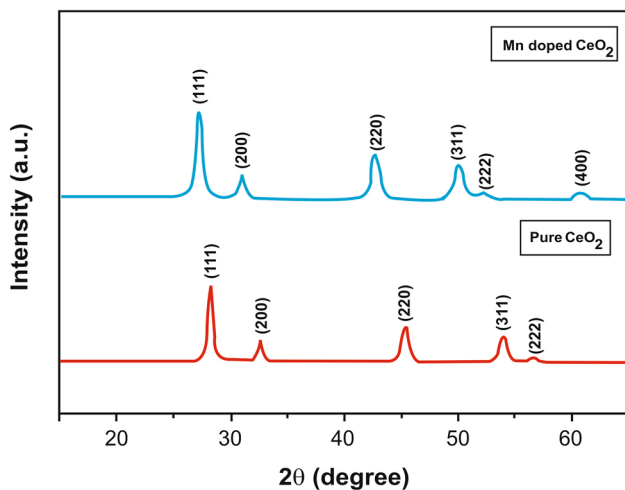


Fig. 1 XRD pattern of pure and Mn-doped CeO₂ nanoparticles

The grain sizes were evaluated from the Scherrer's relation. It showed that increases in the dopant concentration of Mn increased the average grain size. The lattice parameter decreased with increasing the dopant concentration of Mn. It was understood that Mn doping in CeO₂ produced crystal defects around the dopants and the charge imbalance arising from this imperfection changed the stoichiometry of the materials. At lower temperatures, a grain boundary effect was seen in polycrystalline materials, which was characterized by a reduction in dc ionic conductivity with decreasing grain size, i.e., increasing number of grain boundaries per unit length [21].

3.2 FTIR analysis

FTIR spectrum of the pure and the Mn-doped CeO₂ nanoparticles is shown in Fig. 2. Three strong absorption peaks were seen at 3432, 1622 and 682 cm⁻¹. The broad absorption bands at 3432 and 1622 cm⁻¹ could be associated with the symmetric extending (ν O–H) and bending methods of (δ O–H) inside bonded water molecules, respectively. The band at 1622 cm⁻¹ related to anti-symmetric and symmetric stretching modes of the carboxyl group. The bending mode of Ce–O–C (δ) was seen at well below 682 cm⁻¹ which affirmed the formation of CeO₂ without impurities [6]. The comparing lessening in the force of the O–H and C=O modes brought about expanding the of the assimilation band of cubic period of CeO₂, which showed up at 682 cm⁻¹.

3.3 SEM analysis

Scanning electron microscopy (SEM) is one of the most widely used techniques for the characterization of size and

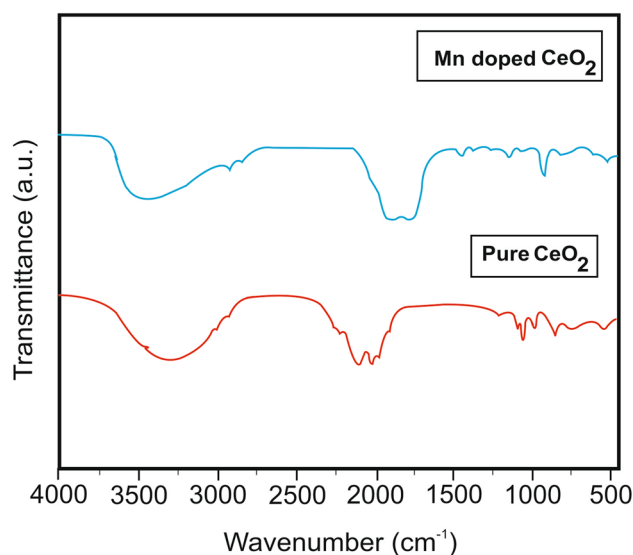


Fig. 2 FTIR spectrum of pure and Mn-doped CeO₂ nanoparticles

morphology of the particles. The SEM pictures of the pure and the Mn-doped CeO₂ nanoparticles are shown in Fig. 3a, b. It is clearly observed that the particles that are highly aggregated are of permeable nature. There are small agglomerated particles and this may be because of the lower calcination temperature. This affirms the decrease in crystalline size essentially by adding Mn particles to CeO₂ host [16].

3.4 Optical studies

The absorption spectrum of the pure and the Mn-doped CeO₂ nanoparticles is shown in Fig. 4. It was seen that the strong absorption peak with broader shoulder could be identified in the wavelength scope of 460 and 475 nm for the pure and the doped samples. It was noticed that the absorption of Ceria in the UV region originated from the charge–transfer transition between the O²⁻(2p) and Ce⁴⁺(4f) orbit in CeO₂. It was found that at the outermost nanocrystals surface, Ce⁴⁺ ions existed together with Ce³⁺ ones; when the cluster sizes diminished, the amount of Ce³⁺ increased [22]. There was also an electrostatic potential impact because of a Cerium valence change, which brought about the blue shift of the band gap. In this manner, the charge transition of Ce particle (Ce³⁺–Ce⁴⁺) might play a vital role in increasing the band gap of Cerium oxide sample. It was seen that the absorption edge shifted towards the lower wavelength side with the increase in the dopant concentration. The wavelength of the maximum excitation absorption decreased as the particle size decreased, due to the result of the quantum confinement of the photo-generated electron–hole pairs. The optical absorption coefficient (α) was calculated from transmittance by using the following relation:

$$\alpha = \frac{1}{d} \log \left(\frac{1}{T} \right), \quad (2)$$

Fig. 3 a, b SEM image of Mn-doped CeO₂ nanoparticles

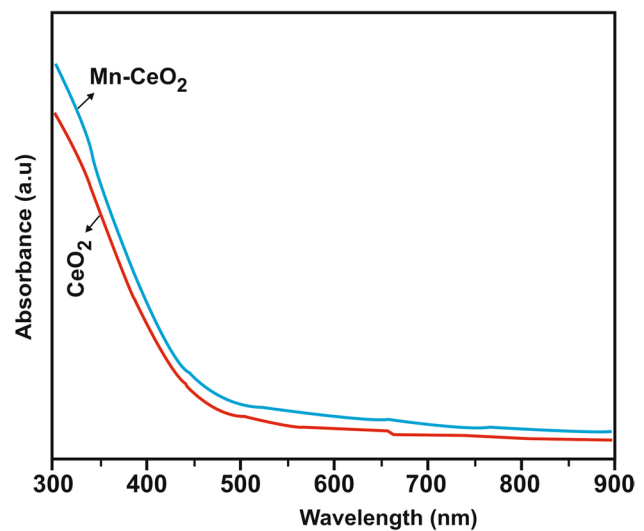
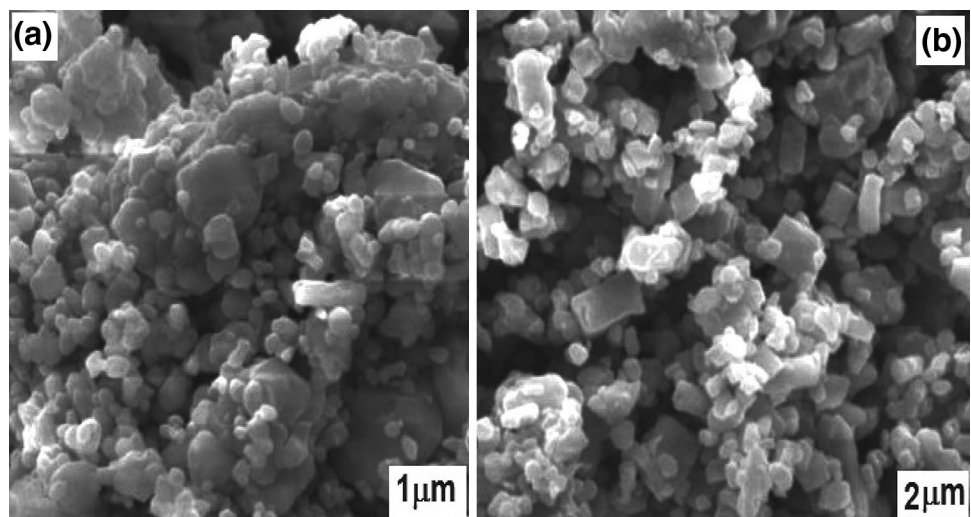


Fig. 4 UV–Visible absorption spectrum of pure and Mn-doped CeO₂ nanoparticles

where T is the transmittance and d is the thickness. The study has an absorption coefficient (α) obeying the following relation for high photon energies ($h\nu$):

$$\alpha = \frac{A(h\nu - E_g)^{1/2}}{h\nu}, \quad (3)$$

where α , E_g and A are the absorption coefficient, band gap and constant, respectively. A plot of variation of $(\alpha h\nu)^2$ versus $h\nu$ is shown in Fig. 5. The band gap of the prepared samples was calculated by extrapolating the rising part of the absorption peak. The evaluated band gap values for the pure and the Mn-doped CeO₂ nanoparticles were observed to be 2.7 and 2.6 eV, respectively. It could be seen that the band gap value slightly decreased when the dopant concentration of Mn was increased.

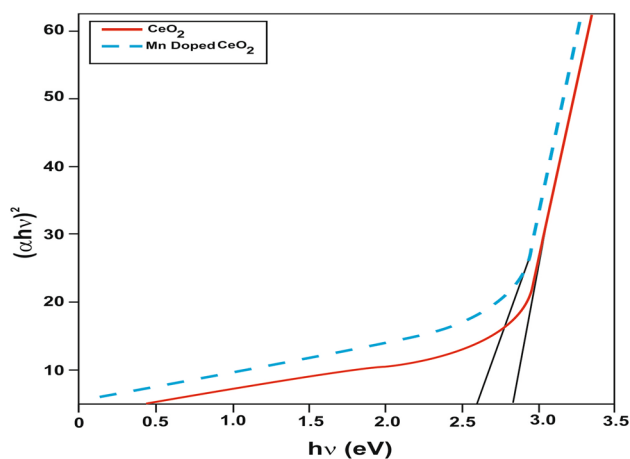


Fig. 5 Plot of $(\alpha h\nu)^2$ versus photon energy of pure and Mn-doped CeO₂ nanoparticles

3.5 Dielectric properties

The pure and the Mn-doped CeO₂ nanoparticle pellets in disk form were examined in different temperatures. For estimations, the samples were obtained with the diameter of ~ 12 mm and thickness ~ 1 mm and a specimen was set between the electrodes with a conventional four-terminal specimen holder for examinations including temperature varieties along with a conventional two-terminal sample for just surrounding conditions. The sample was mounted between copper platforms and electrodes. The faces were coated with the silver paint for the purpose of ensuring great electrical contact. The capacitance and the dissipation factor of the parallel plate capacitor formed by the copper plate and the terminal having the specimen as a dielectric medium were measured. The dielectric constant and the dielectric loss of the pure and the Mn-doped CeO₂ nanoparticles were studied at different temperatures in the frequency region 50 Hz–5 MHz. The dielectric constant was evaluated by using the following relation:

$$\epsilon_r = \frac{Cd}{\epsilon_0 A}, \quad (4)$$

where d and A are the thickness and the area of the Mn-doped CeO₂ sample, respectively. The dielectric constant was measured for the Mn-doped CeO₂ nanoparticles as a function of the frequency at various temperatures as appeared in Fig. 6. The strength of the frequency dependence in the lower frequency region is clear. The dielectric constant diminished with the increase in the frequency and as a result it became constant at high frequencies [23]. The higher value of the dielectric constant can also be explained on the basis of interfacial/space charge polarization because of inhomogeneous dielectric structure. The inhomogeneities

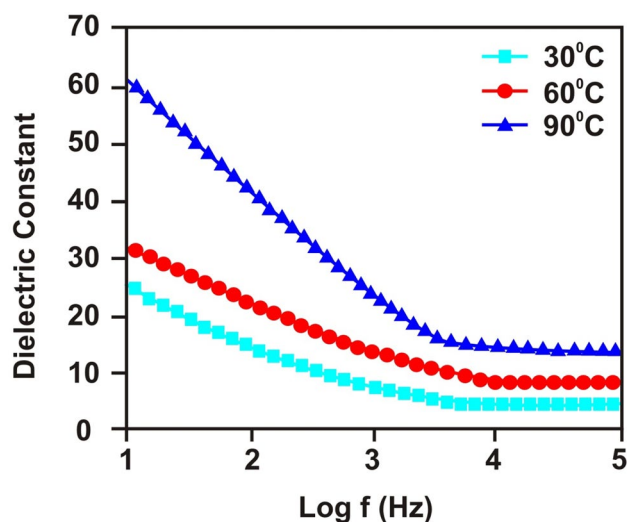


Fig. 6 Dielectric constant of Mn-doped CeO₂ nanoparticles

present in the system might be porosity and grain structure. The polarization got diminished with the increase in the frequency and after that it achieved a consistent value. This was due to the fact that beyond a certain frequency of the external field the hopping between different metal ions (Mn⁺³ and Mn⁺⁴) could not follow the alternating field. As the dopant concentration was increased, there were more manganese ions and so the dielectric polarization also got decreased, which in turn decreased the dielectric constant. Figure 7 shows the dielectric loss versus $\log f$ for various temperatures for the Mn doped CeO₂ nanoparticles. It can be seen that the dielectric loss gets reduced with the increase in the frequency for all temperatures, which may be due to the space charge polarization [24]. It is also understood that the dielectric loss was reduced by increasing the frequency

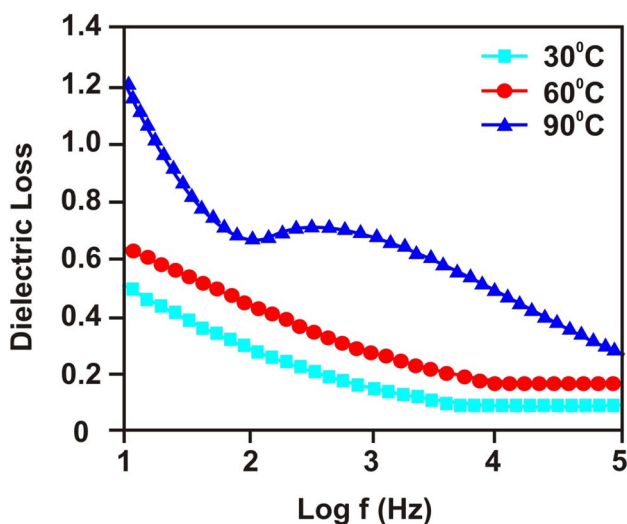


Fig. 7 Dielectric loss of Mn-doped CeO₂ nanoparticles

and it became low at high-frequency region. It shows the capability of these materials to be used in high-frequency device applications [25].

3.6 AC conductivity measurement

The ac conductivity plot of the pelletized form of pure and Mn-doped CeO₂ nanoparticles was studied. It could be observed that the ac conductivity gradually increased with increase in the frequency of the applied ac field because the increase in the frequency would enhance the electron hopping frequency. The ac conductivity of the Mn-doped CeO₂ nanoparticles could be calculated by the following relation:

$$\sigma_{ac} = 2\pi\epsilon_0\epsilon_r f \tan \delta, \quad (5)$$

where ϵ_0 is permittivity in free space, ϵ_r is dielectric constant, f is the frequency and $\tan \delta$ is the loss factor. The ac conductivity of Mn-doped CeO₂ nanoparticles is shown in Fig. 8. There is a small increase in the electrical conductivity of the nanomaterial at the low-frequency region for an increase in the frequency and is the same for all temperatures. Conversely, at high frequencies, particularly in the KHz area, there appears a sudden increment in the conductivity and it is enormous at high temperatures which could be ascribed to small polaron jumping. It is observed that the frequency-independent behavior at lower frequency region which characterizes the dc conductivity and the dispersion at higher-frequency region shows the frequency-dependent behavior. It is consistent with the increase in temperature resulting in enormous carrier hopping that causes the increase in the conductivity. An analysis of the conducting mechanism of pure and Mn-doped CeO₂ nanoparticles reveals that σ_{ac} varies clearly with the temperature. The

values of activation energy of the pure and the Mn-doped CeO₂ nanoparticles were found to be 0.24 and 0.22 eV, respectively. The activation energy may depend on many parameters like ionic radii of the constituent ions, lattice parameters, surface atoms and grain boundaries [26]. The electronic conductivity of the nanocrystalline cerium oxide was increased as compared with the undoped cerium oxide, which is explained by a donor effect of grain boundaries. Such a donor effect may originate from an enhanced reduction at the grain boundaries as compared with the bulk. In fact, reduced activation energy for the electronic conductivity as compared with the single crystal value was found and attributed to a decrease in the enthalpy of reduction of nanocrystalline CeO_{2-x} [21].

4 Conclusion

By adopting co-precipitation method Mn-doped CeO₂ nanoparticles were prepared. The formation of Mn-doped CeO₂ nanoparticles was confirmed by X-ray diffraction. From the XRD and FT-IR analysis, it was identified that the obtained nanopowders were in single phase cubic structure with average grain sizes of 12 and 14 nm for the pure and doped samples. The SEM observation clearly showed the fact that the particles were strongly aggregated and appeared in porous morphology. UV-visible spectrum revealed that both the pure and Mn-doped particle absorption occurred at the UV region. UV-visible absorption studies showed that the decrease of particle size was accompanied by decreasing the band gap value band gap is reduced from 2.7 to 2.7 eV (should be 2.6 eV) for Mn doping. Analysis pertaining to the variations of the dielectric constant, the dielectric loss and AC conductivity with frequency and temperature for the pure and Mn-doped CeO₂ nanoparticles was performed. The dielectric studies revealed that both the dielectric constant and the dielectric loss varied inversely, i.e., (decreased) with the frequency. The dielectric constant suddenly dropped at lower frequencies. On account of the interfacial/space polarization, the Mn dopant concentration was increased more by decreasing the dielectric polarization, which in turn decreased the dielectric constant. Dielectric loss of the pure and Mn-doped CeO₂ samples was found to decrease with the increase in frequency. It could be possible because of the interfacial/space charge polarization effect. When Mn dopant concentration was increased, the dielectric constant value became low. The AC electrical conductivity was found to increase with an increase in the temperature and the frequency. The ac conductivity decreased with the increase in dopant concentration, which could be attributed to the fact that the dopants introduced the defect ions (such as tin interstitials and oxygen vacancies) in CeO₂ system.

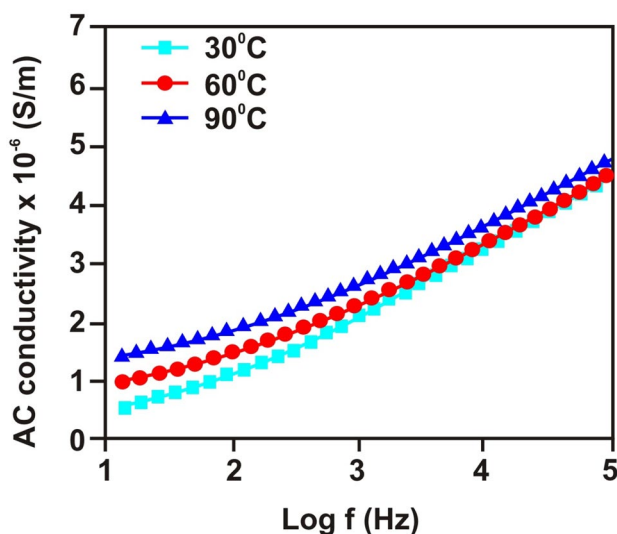


Fig. 8 Variation of ac conductivity of Mn-doped CeO₂ nanoparticles

References

1. A. Bumajdad, J. Eastoe, A. Mathew, *Adv. Colloid Interf. Sci* **147–148**, 56–66 (2009)
2. N.J. Lawrence, J.R. Brewer, L. Wang, T. Wu, T. -sing, J. Wellskingsbury, M.M. Ihrig, G. Wang, Y. Soo, W. Mei, C. -ning Cheung, *Nano Lett.* **11**, 2666–2671 (2011)
3. S. Sato, R. Takafhashi, M. Kobune, H. Gotoh, *Appl. Catal. A: Gen* **356**, 57–63 (2009)
4. Q. Yuan, H.H. Duan, L.L. Li, L.D. Sun, Y.W. Zhang, C.H. Yan, *J. Colloid Interf. Sci* **335**, 151–167 (2009)
5. H. Chen, H. Chang, *Colloid Surf. A. Physicochem. Eng. Asp.* **242**, 61–69 (2004)
6. M.G. Sujana, K.K. Chattopadyay, S. Anand, *Appl. Surf. Sci* **254**, 7405–7409 (2008)
7. W. Fuxing, W. Zhifeng, W. Maoyan, G. Xunda, W. Chunhong, M.J. Zhang, *Rare Earth* **28**, 139–143 (2010)
8. Q.Y. Wen, H.W. Zhang, Q.H. Yang et al., *J. Appl. Phys* **107**, 09C307 (2010)
9. L. Bi, H.S. Kim, G.F. Dionne et al., *J. Appl. Phys.* **103**, 07D138 (2008)
10. S. Kumar, Y.J. Kim, B.H. Koo, *J. Nanosci. Nanotechnol.* **10**, 7204 (2010)
11. D. Tian, C. Zeng, Y. Fu, H. Wang, H. Luo, C. Xiang, Y. Wei, K. Li, X. Zhu, *Solid State Commun.* **231–232**, 68–79 (2016)
12. Y.H. Tang, H. Zhang, L. Cui, et al., *Phys. Rev. B* **82**, 125104 (2010)
13. Z.X. Yang, T.K. Woo, K. Hermansson, *J. Chem. Phys.* **124**, 2247004 (2006)
14. G. Dutta, S.K. Saha, U.V. Waghmare, *Solid State Commun.* **150**, 2020–2022 (2010)
15. D. Tian, C. Zeng, H. Wang, H. Luo, X. Cheng, C. Xiang, Y. Wei, K. Li, X. Zhu, *J. Alloy. Compd.* **671**, 208–219 (2016)
16. J. Choi, D. Amaranatha Reddy, M. Jahurul Islam, R. Ma, T.K. Kim, *J. Alloy. Compd.* **688**, 527–e536 (2016)
17. R. Ma, Y. Kim, D. Amaranatha Reddy, T.K. Kim, *Ceramics Int.* (2015), <https://doi.org/10.1016/j.ceramint.2015.06.086>
18. N.J. Islam, D. Amaranatha Reddy, J. Choi, T. KIM, *RSC Adv.* (2016). <https://doi.org/10.1039/C5RA27533D>
19. A. Doaga, A.M. Cojocariu, W. Amin, F. Heib, P. Bender, R. Hempelmann, O.F. Caltun, *Mater. Chem. Phys.* **143**(1), 305–310 (2013)
20. S. Gnanam, V. Rajendran, *J. Sol Gel Sci. Technol.* **58**, 62–69 (2011)
21. A. Tschõpe, E. Sommer, R. Birringer, *Solid State Ionics* **139**, 255–265 (2001)
22. P. Patsalas, S. Logothetidis, C. Metaxa, *Appl. Phys. Lett.* **81**, 466 (2002)
23. S. Suresh, *Appl. Nanosci.* **4**, 325–329 (2014)
24. S. Suresh, C. Arunseshan, *Appl. Nanosci.* **4**, 179–184 (2014)
25. S. Sagadevan, *J. Nano. Res.* **34**, 91–97 (2015)
26. S. Sagadevan, J. Podder, *Mater. Res.* **19**, 420–425 (2016)